## Supporting Information for

# Boosting the sintering resistance of platinum-alumina catalyst via a morphology-confined phosphate doping strategy

Jinshi Dong, Yutao Zhang, Hongji Zou, Panpan Chang *, Yan Guo *

School of Biological and Chemical Engineering, Guangxi University of Science and Technology, Liuzhou 545006, Guangxi, China

*Corresponding author. E−mail: changpp@gxust.edu.cn (P. Chang); guoyan56@hotmail.com (Y. Guo).

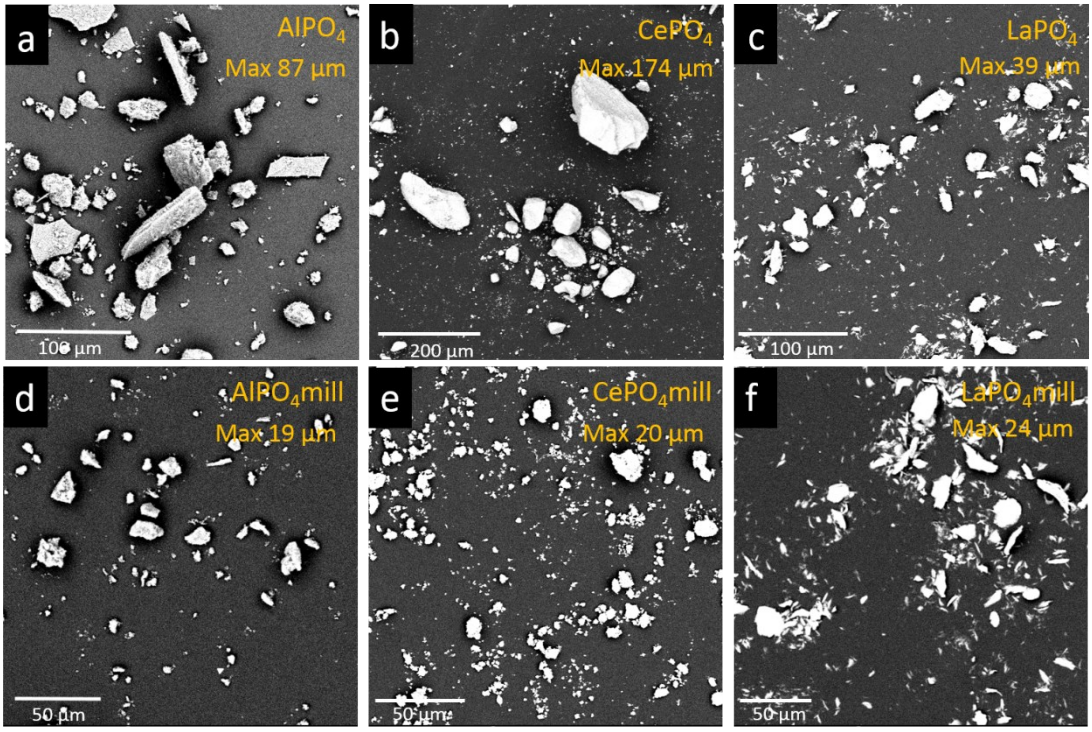


Fig. S1. SEM images of (a-c) $MPO_4$ and (d-f) $MPO_4$mill.

Table S1 ICP results of Pt loadings for various catalysts [a].

| Sample | Pt loading (wt.%) |
|---|---|
| Pt-$Al_2O_3$-400 | 0.77 |
| Pt-$Al_2O_3$-800 | 0.77 |
| Pt-$Al_2O_3$-1000 | 0.75 |
| Pt-$AlPO_4$-400 | 0.76 |
| Pt-$CePO_4$-400 | 0.75 |
| Pt-$LaPO_4$-400 | 0.75 |
| Pt-$AlPO_4$mill-400 | 0.76 |
| Pt-$CePO_4$mill-400 | 0.74 |
| Pt-$LaPO_4$mill-400 | 0.75 |
| Pt-($Al_2O_3$+$AlPO_4$)mill-400 | 0.75 |
| Pt-($Al_2O_3$+$CePO_4$)mill-400 | 0.73 |
| Pt-($Al_2O_3$+$LaPO_4$)mill-400 | 0.77 |

[a] Pt-$Al_2O_3$-$MPO_4$-400 and Pt-$Al_2O_3$-$MPO_4$mill-400 catalysts were not measured because of their precise mixing Pt-$Al_2O_3$ with $MPO_4$ or $MPO_4$mill at the weight ratio of 2: 1.

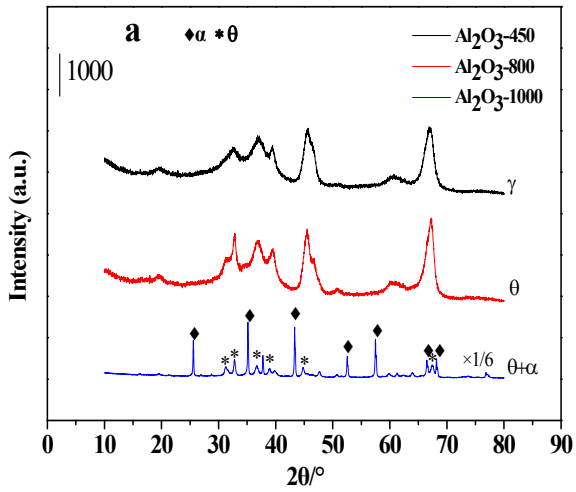


Fig. S2. XRD patterns of $Al_2O_3$ calcinated at different temperatures.

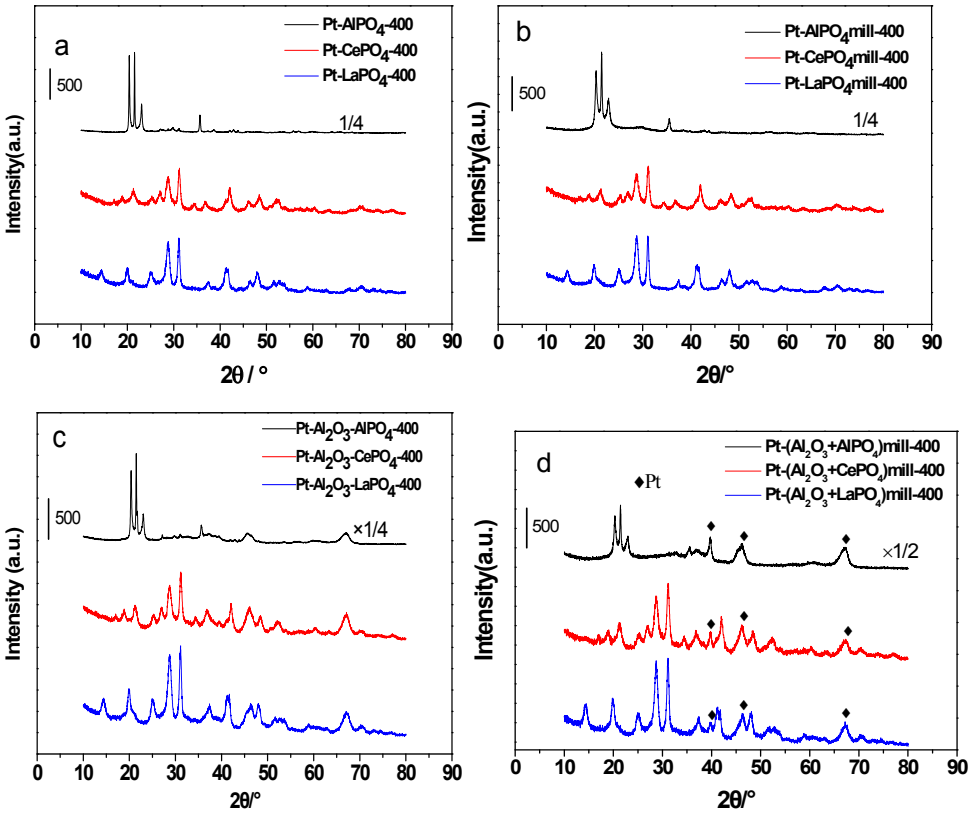


Fig. S3. XRD patterns of the fresh catalysts.

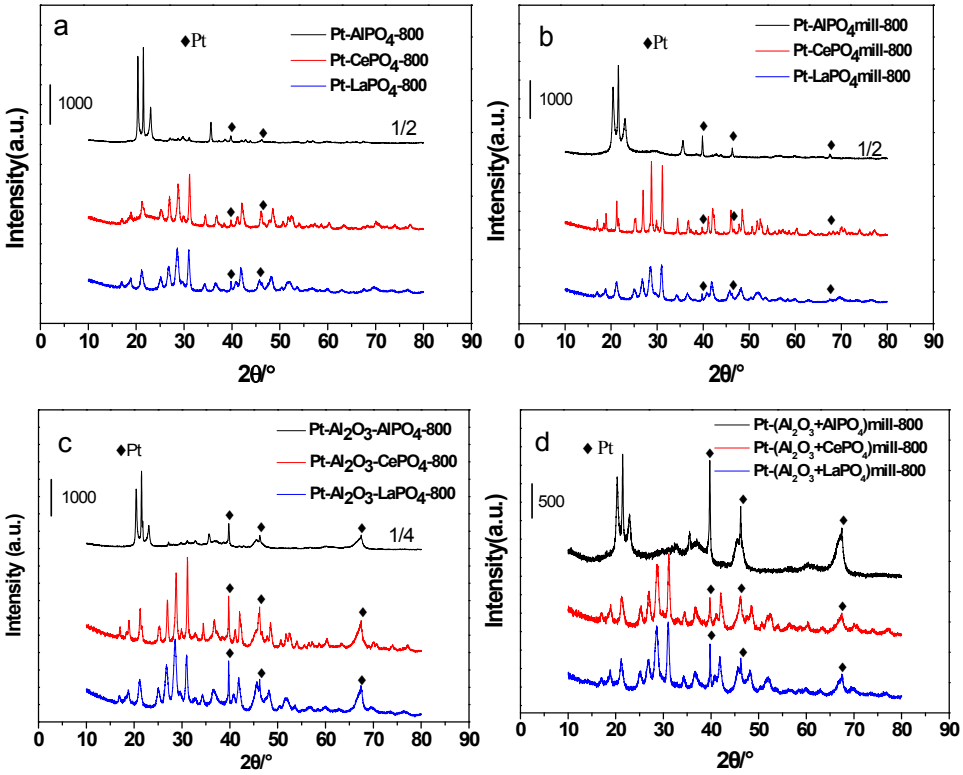


Fig. S4. XRD patterns of the 800 °C aged catalysts.

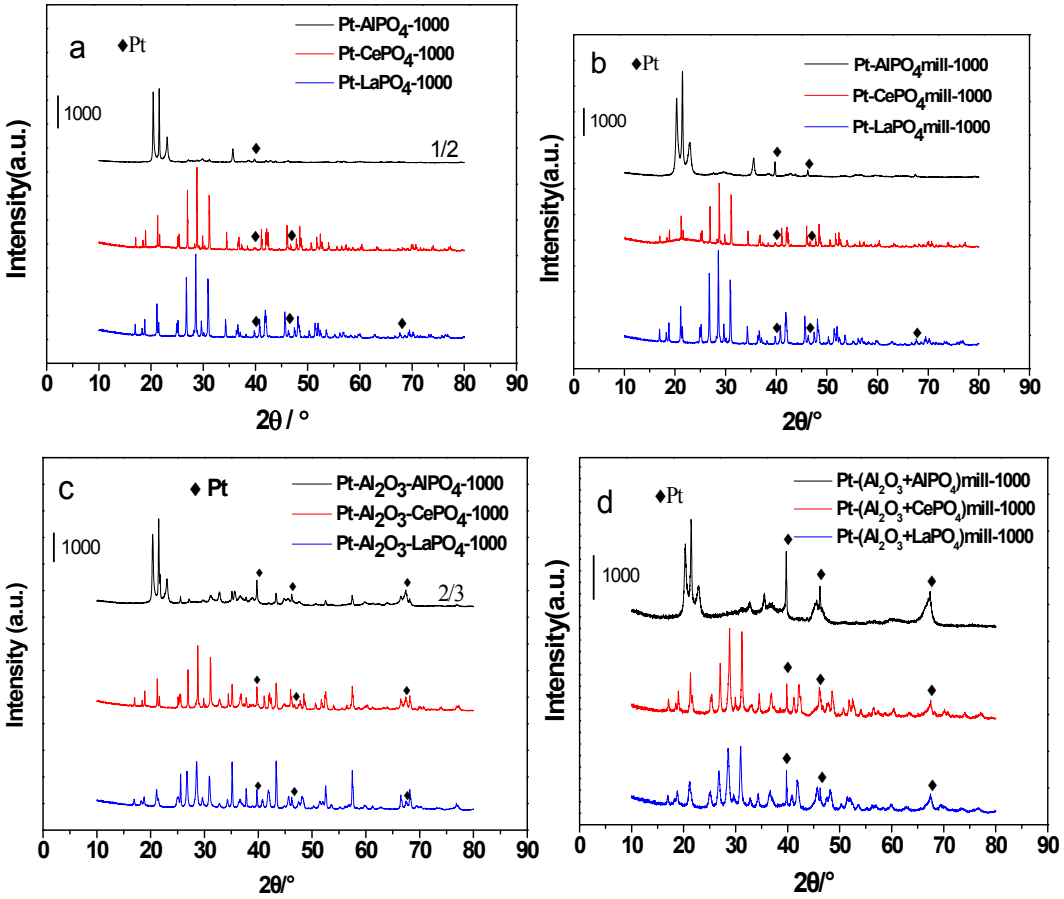


Fig. S5. XRD patterns of the 1000 °C aged catalysts.

Table S2 The components and phases detected by XRD.

| Sample | Fresh (400 °C) | Aged (800 °C) | Aged (1000 °C) |
|---|---|---|---|
| Pt-$Al_2O_3$ | γ [a] | θ | α+θ |
| Pt-$AlPO_4$ | $AlPO_4$ | $AlPO_4$+Pt | $AlPO_4$+Pt |
| Pt-$CePO_4$ | $CePO_4$ | $CePO_4$+Pt | $CePO_4$+Pt |
| Pt-$LaPO_4$ | $LaPO_4$ | $LaPO_4$-M[b]+Pt | $LaPO_4$-M+Pt |
| Pt-$AlPO_4$mill | $AlPO_4$ | $AlPO_4$+Pt | $AlPO_4$+Pt |
| Pt-$CePO_4$mill | $CePO_4$ | $CePO_4$+Pt | $CePO_4$+Pt |
| Pt-$LaPO_4$mill | $LaPO_4$ | $LaPO_4$-M+Pt | $LaPO_4$-M+Pt |
| Pt-$Al_2O_3$-$AlPO_4$ | $AlPO_4$+γ | $AlPO_4$+θ+Pt | $AlPO_4$+θ+α+Pt |
| Pt-$Al_2O_3$-$CePO_4$ | $CePO_4$+γ | $CePO_4$+θ+Pt | $CePO_4$+θ+α+Pt |
| Pt-$Al_2O_3$-$LaPO_4$ | $LaPO_4$+γ | $LaPO_4$+θ+Pt | $LaPO_4$+θ+α+Pt |
| Pt-$Al_2O_3$-$AlPO_4$mill | $AlPO_4$+γ | $AlPO_4$+θ+Pt | $AlPO_4$+θ+Pt |
| Pt-$Al_2O_3$-$CePO_4$mill | $CePO_4$+γ | $CePO_4$+θ+Pt | $CePO_4$+θ+Pt |
| Pt-$Al_2O_3$-$LaPO_4$mill | $LaPO_4$+γ | $LaPO_4$+θ+Pt | $LaPO_4$+θ+Pt |
| Pt-($Al_2O_3$+$AlPO_4$)mill | $AlPO_4$+γ+Pt | $AlPO_4$+θ+Pt | $AlPO_4$+θ+Pt |
| Pt-($Al_2O_3$+$CePO_4$)mill | $CePO_4$+γ+Pt | $CePO_4$+θ+Pt | $CePO_4$+θ+Pt |
| Pt-($Al_2O_3$+$LaPO_4$)mill | $LaPO_4$+γ+Pt | $LaPO_4$+θ+Pt | $LaPO_4$+θ+Pt |

[a] The Greeks stand for the phases of $Al_2O_3$; [b] $LaPO_4$-M stands for monoclinic $LaPO_4$ while the initial $LaPO_4$ is hexagonal.

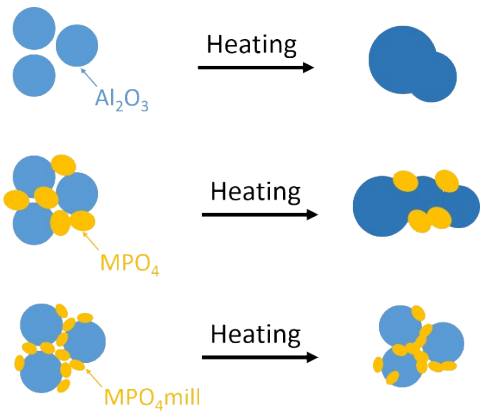


Scheme S1 The inhibition mechanism for $Al_2O_3$ phase transformation by $MPO_4$ upon heating.

Table S3 The 50% and 100% conversion temperatures ($T_{50}$ and $T_{100}$) of CO oxidation for the fresh and aged catalysts **without** $H_2$ reduction.

| Sample | Fresh (400 °C) | Aged (800 °C) | Aged (1000 °C) |
|---|---|---|---|
| Pt-$Al_2O_3$ | 257[a]/263[b] | 378/388 | 364/384 |
| Pt-$AlPO_4$ | 273/286 | 400/447 | 470/552 |
| Pt-$CePO_4$ | 260/273 | 370/382 | 536/603 |
| Pt-$LaPO_4$ | 252/272 | 423/443 | 427/472 |
| Pt-$AlPO_4$mill | 250/268 | 329/339 | 376/404 |
| Pt-$CePO_4$mill | 259/267 | 316/354 | 387/409 |
| Pt-$LaPO_4$mill | 238/248 | 325/336 | 383/396 |
| Pt-$Al2O_3$-$AlPO_4$ | 272/275 | 384/395 | 403/420 |
| Pt-$Al_2O_3$-$CePO_4$ | 271/288 | 373/397 | 388/402 |
| Pt-$A_2O_3$-$LaPO_4$ | 274/282 | 385/399 | 376/390 |
| Pt-$Al_2O_3$-$AlPO_4$mill | 289/303 | 350/358 | 350/375 |
| Pt-$Al_2O_3$-$CePO_4$mill | 291/296 | 345/362 | 344/367 |
| Pt-$Al_2O_3$-$LaPO_4$mill | 295/302 | 348/362 | 352/360 |
| Pt-($Al_2O_3$+$AlPO_4$)mill | 300/310 | 333/354 | 401/424 |
| Pt-($Al_2O_3$+$CePO_4$)mill | 285/297 | 352/362 | 354/369 |
| Pt-($Al_2O_3$+$LaPO_4$)mill | 292/303 | 318/335 | 337/357 |

[a]$T_{50}$ (°C); [b]$T_{100}$ (°C).

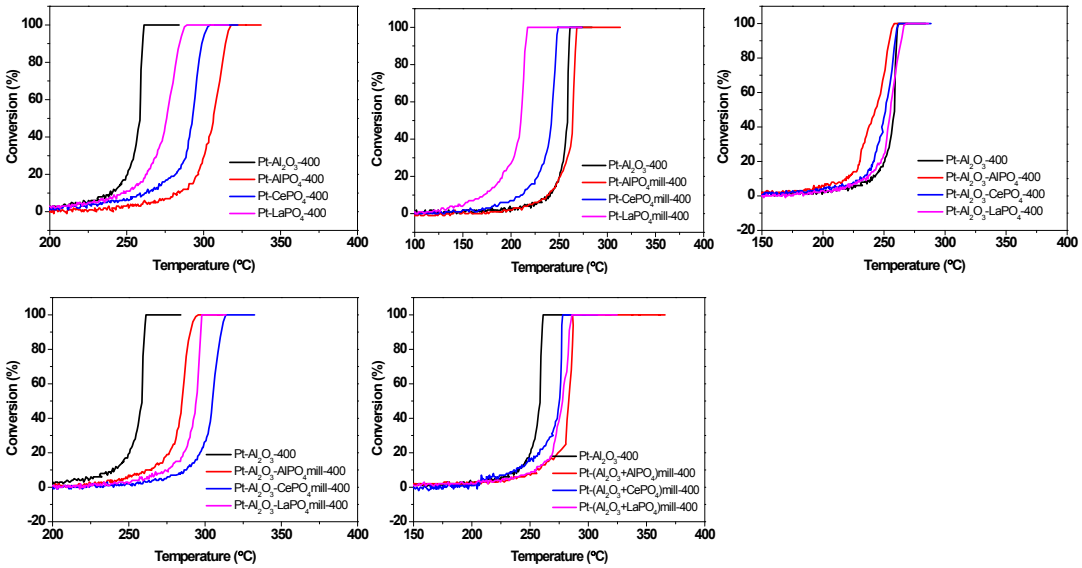


Fig. S6. CO oxidation light-off profiles of the fresh catalysts after $H_2$ reduction (300 °C, in 5% $H_2$/Ar). Feed gas stream: 1% CO and 2% $O_2$ balanced with Ar, flow rate: 500 mL/min. All samples were kept ~0.38 mg Pt by varying different amounts of catalysts.

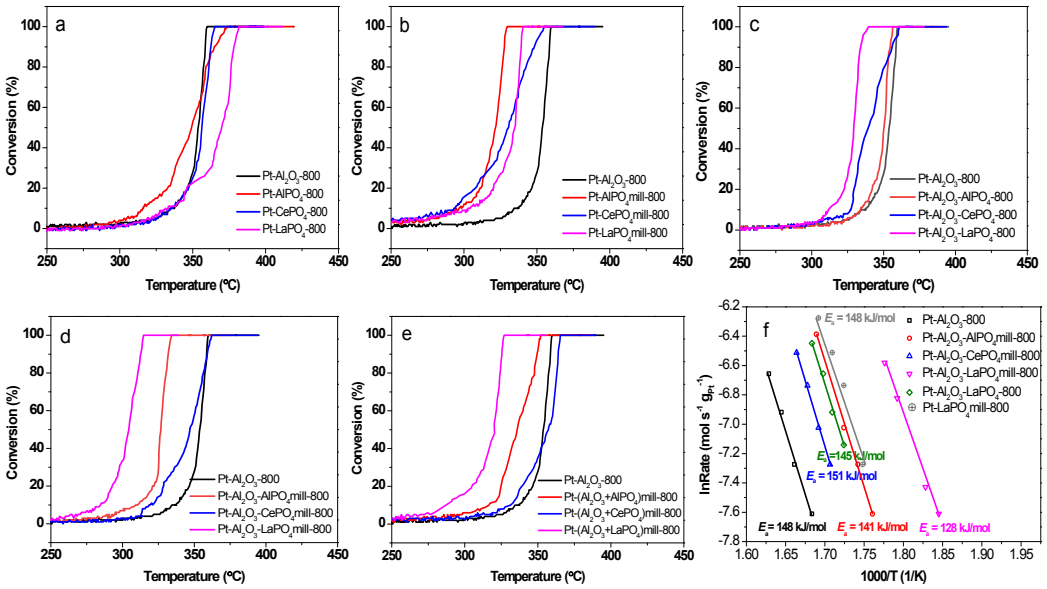


Fig. S7. (a-e) CO oxidation light-off profiles and (f) Arrhenius plots of the 800 °C aged catalysts after $H_2$ reduction (300 °C, in 5% $H_2$/Ar). Activity tests feed gas stream: 1% CO and 2% $O_2$ balanced with Ar, flow rate: 500 mL/min. All samples were kept ~0.38 mg Pt by varying different amounts of catalysts.

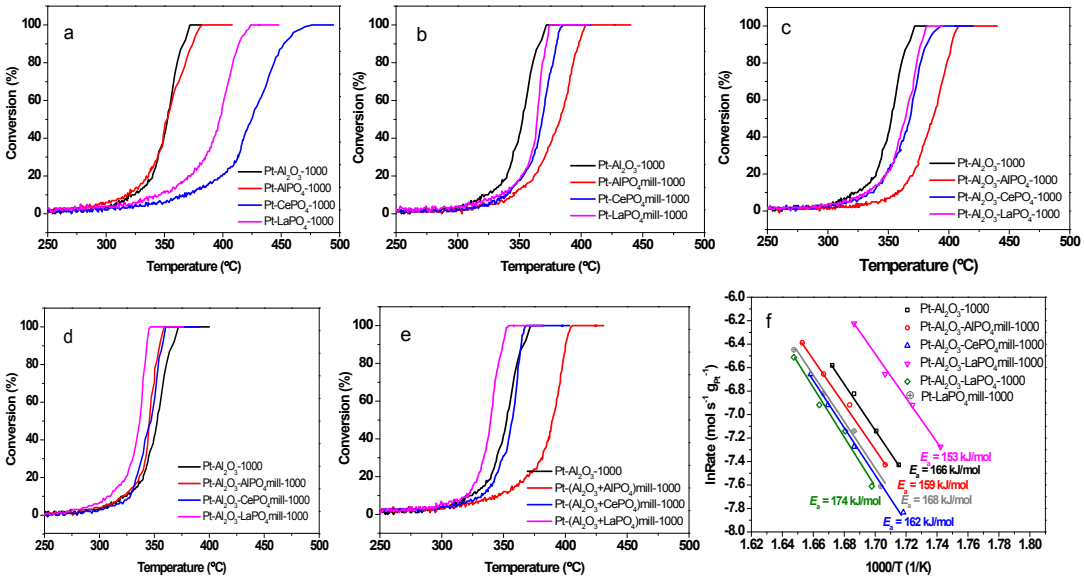


Fig. S8. (a-e) CO oxidation light-off profiles and (f) Arrhenius plots of the 1000 °C aged catalysts after $H_2$ reduction (350 °C, in 5% $H_2$/Ar). Activity tests feed gas stream: 1% CO and 2% $O_2$ balanced with Ar, flow rate: 500 mL/min. All samples were kept ~0.38 mg Pt by varying different amounts of catalysts.

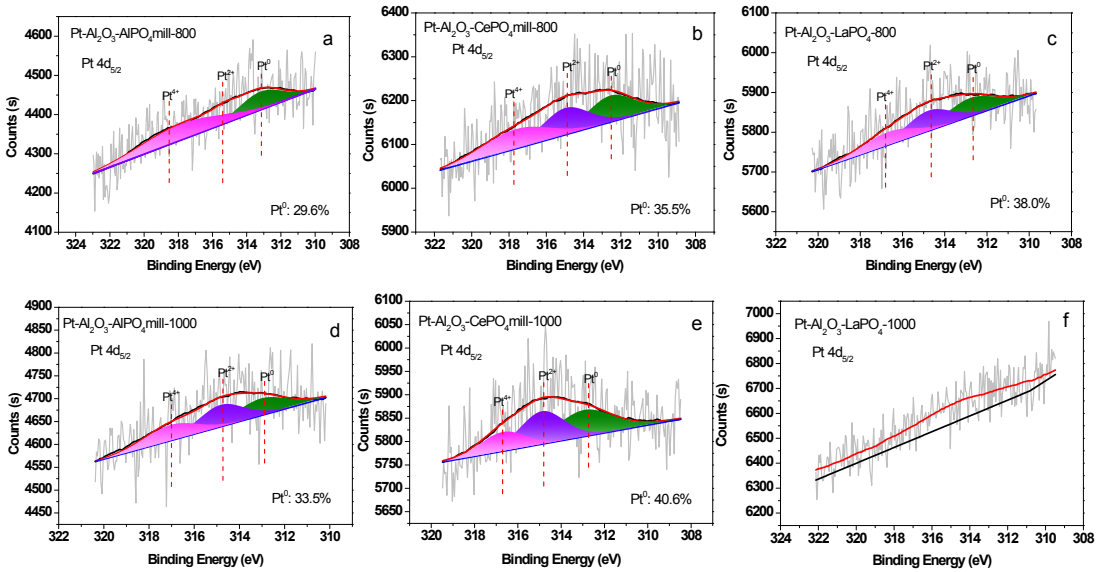


Fig S9. XPS spectra of (a,b, c) 800°C and (e, d, f) 1000 °C aged catalysts after $H_2$ reduction. Blue lines are background data, light gray lines are raw data and red lines are the fitting results of raw data.

Table S4 Comparison of the CO oxidation rates per platinum atom site (turnover frequency, TOF) for various platinum based catalysts (fresh samples) from literature and in this work.

| Sample | Loading (wt %) | GHSV (L $g_{cal}^{-1}$ $h^{-1}$) | Temperature (°C) | TOF ($s^{-1}$) | Ref. |
|---|---|---|---|---|---|
| Pt-$Al_2O_3$ | 0.77 | 600 (1%) [a] | 250 | 1.15 | this work |
| Pt-$LaPO_4$mill | 0.75 | 600 (1%) | 200 | 1.06 | this work |
| Pt/$CeO_2$ | 0.5 | / | 200 | 0.60 | [1] |
| Pt/$MnO_2$ | 0.5 | / | 200 | 0.53 | [1] |
| Pt/NiO | 0.5 | / | 200 | 1.12 | [1] |
| Pt/$Fe_2O_3$ | 0.5 | / | 200 | 0.15 | [1] |
| Pt/m-$Al_2O_3$-$H_2$ | 0.2 | 48 (2.5%) | 200 | 0.023 | [2] |
| Pt/m-$Al_2O_3$-$H_2$ | 0.2 | 48 (2.5%) | 250 | 0.175 | [2] |
| Commer. Pt/$Al_2O_3$ | 5.0 | 48 (2.5%) | 200 | 0.443 | [2] |
| Pt/θ-$Al_2O_3$ | 0.18 | / (3.7%) | 200 | 0.013 | [3] |
| Pt/θ-$Al_2O_3$ | 0.18 | / (3.7%) | 251 | 0.187 | [3] |
| Pt/$Al_2O_3$-$CeO_2$ | 1.0 | 232.5 (1.9%) | 225 | 0.17 | [4] |
| Pt/α-$Al_2O_3$ | 5.0 | / (1%) | 150 | 0.22 | [5] |
| $PtO_x$/KLTL | 1.0 | / (1%) | 150 | 0.012 | [6] |
| $Pt(NH_3)_4^{2+}$/KLTL | 1.0 | / (1%) | 150 | 0.0038 | [6] |
| Pt-O-Pt/$CeO_2$ | 0.27 | 2400 (0.1%) | 150 | 1.97 | [7] |

[a] The data in () are the volume concentrations of CO in the feed gases. The dispersions measured by CO-chemisorption for Pt-$Al_2O_3$-400 and Pt-$LaPO_4$mill-400 were 32.3% and 49.7%, respectively.

Table S5 $T_{50}$ and $T_{100}$ of CO oxidation reaction for the aged Pt-$Al_2O_3$-$LaPO_4$mill catalysts with different mix ratios (after $H_2$ reduction).

| Sample | 800℃ aged | 1000℃ aged |
|---|---|---|
| Pt-$Al_2O_3$-$LaPO_4$mill-(1:1) | 329/343 | 352/368 |
| Pt-$Al_2O_3$-$LaPO_4$mill-(2:1) | 304/315 | 337/347 |
| Pt-$Al_2O_3$-$LaPO_4$mill-(4:1) | 354/366 | 364/376 |

[a]$T_{50}$ (°C); [b]$T_{100}$ (°C).

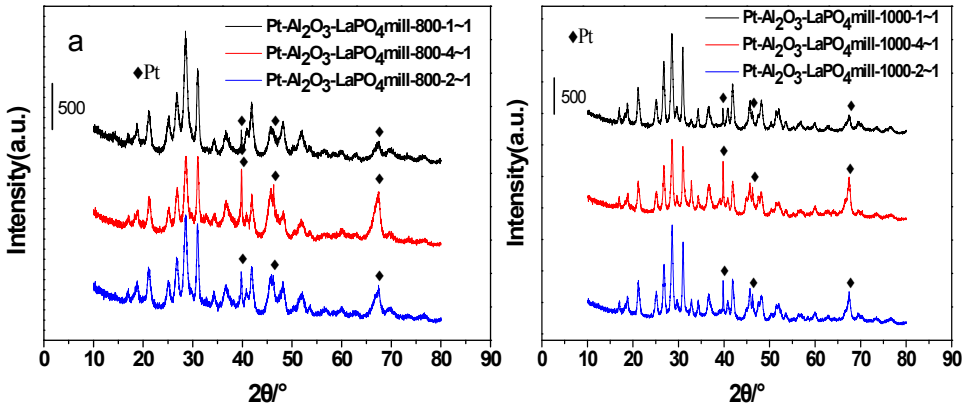


Fig. S10. XRD patterns of the aged Pt-$Al_2O_3$-$LaPO_4$mill catalysts with different mix ratios. The intensity of Pt corresponds to its particle size.

Table S6 BET surface areas ($m^2\ g^{-1}$) and reaction rate ($mmol_{CO}\ s^{-1}\ g_{Pt}^{-1}$) of the Pt-$Al_2O_3$-$LaPO_4$mill catalysts with different mix ratios.

| Sample | BET 400℃ fresh | BET 800℃ aged | BET 1000℃ aged | reaction rate [a] |
|---|---|---|---|---|
| Pt-$Al_2O_3$-$LaPO_4$mill-(1:1) | 100 | 89 | 63 | 0.69 |
| Pt-$Al_2O_3$-$LaPO_4$mill-(2:1) | 119 | 101 | 68 | 2.08 |
| Pt-$Al_2O_3$-$LaPO_4$mill-(4:1) | 132 | 107 | 72 | 0.50 |

[a] Calculated by the reaction rates all at 325 °C.

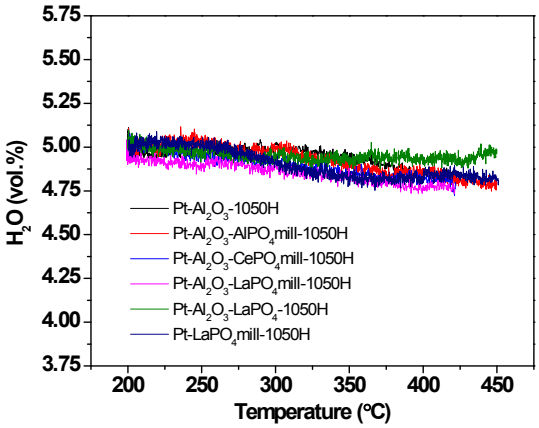


Fig. S11. The changes of $H_2O$ contents with elevated temperatures during the CO oxidation reactions with 5% $H_2O$.

Table S7 BET surface areas ($m^2 g^{-1}$) of the 1050 °C hydrothermally aged catalysts.

| Sample | BET ($m^2 g^{-1}$) |
|---|---|
| Pt-$Al_2O_3$-1050H | 15 |
| Pt-$Al_2O_3$-$AlPO_4$mill-1050H | 67 |
| Pt-$Al_2O_3$-$CePO_4$mill-1050H | 52 |
| Pt-$Al_2O_3$-$LaPO_4$mill-1050H | 56 |
| Pt-$LaPO_4$mil-1050H | 12 |
| Pt-$Al_2O_3$-$LaPO_4$-1050H | 28 |

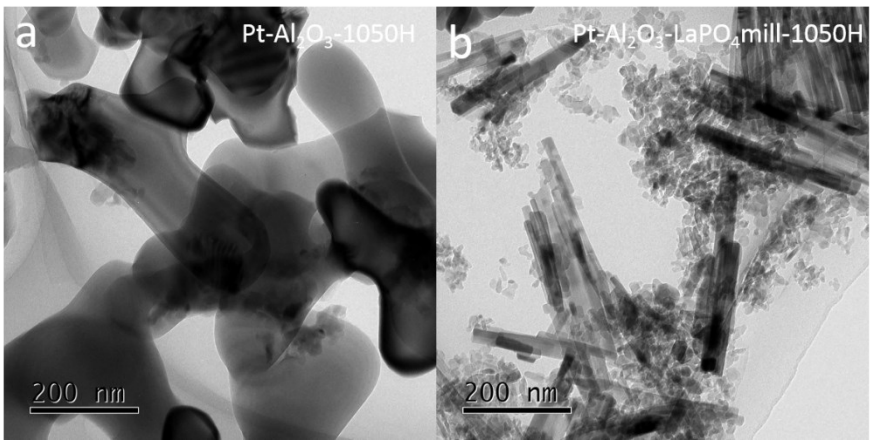


Fig. S12. TEM images of (a) Pt-$Al_2O_3$-1050H and (b) Pt-$Al_2O_3$-$LaPO_4$mill-1050H.

## References

[1] An, K., et al. Enhanced CO Oxidation Rates at the Interface of Mesoporous Oxides and Pt Nanoparticles. *J. Am. Chem. Soc.* **2013**, *135*, 16689-16696.

[2] Zhang, Z. et al. Thermally stable single atom Pt/m-$Al_2O_3$ for selective hydrogenation and CO

oxidation. *Nat. Commun.* **2017***,* 8, 16100.
[3] Moses-DeBusk, M. *et al.* CO oxidation on supported single Pt atoms: experimental and ab initio density functional studies of CO interaction with Pt atom on theta-$Al_2O_3$(010) surface. *J. Am. Chem. Soc.* **2013**, 135, 12634-12645.
[4] Jones, J. et al. Thermally stable single-atom platinum-on-ceria catalysts via atom trapping. Science **2016**, 353, 150-154.
[5] Kale, M. J., Christopher P. Utilizing quantitative in situ FTIR spectroscopy to identify wellcoordinated Pt atoms as the active site for CO oxidation on $Al_2O_3$-supported Pt catalysts. ACS Catal. **2016**, 6, 5599-5609.
[6] Kistler, J. D. et al. A single-site platinum CO oxidation catalyst in zeolite KLTL: microscopic and spectroscopic determination of the locations of the platinum atoms. *Angew. Chem. Int. Ed.* **2014**, 53, 8904-8907.
[7] Wang, H., et al. Surpassing the single-atom catalytic activity limit through paired Pt-O-Pt ensemble built from isolated Pt1 atoms. Nat. Commun. **2019**, 10, 3808.